Iranian Journal of Materials Science and Engineering, Vol. 19, Number 4, December 2022
RESEARCH PAPER

A Study on Durability Performance of Concretes Incorporating Graphene Oxide Nanoplatelets and Ground Granulated Blast Furnace Slag

D. Rezakhani, A. H. Jafari*

* *jafham2020@gmail.com*

Materials Science and Engineering Dept., Shahid Bahonar University

Received: March 2022 Revised: June 2022 Accepted: August 2022
DOI: 10.22068/ijmse.2725

Abstract: *In this work, the addition of a combination of Graphene Oxide Nanoplatelets (GONPs) and Ground Granulated Blast Furnace Slag (GGBFS) was studied as admixture in concrete. Tests on physical and mechanical properties and chloride permeability were conducted. GGBFS was replaced with Ordinary Portland Cement (OPC) and it was determined that GGBFS Up to 50% by weight improves the physical and mechanical properties of concrete. GONPs with an optimal amount of 50% by weight of GGBFS were added to the concrete and the physical and mechanical properties of the samples were determined. It was observed that the addition of GONPs was effective in improving the mechanical strength and physical properties of specimens. The results indicated that addition of 0.1 wt.% GO and 50 wt.% GGBFS would increase the compressive strength of the concrete sample up to 42.7% during 28 days and 46% during 90 days compared to OPC. Concrete with a combination of 0.1 wt.% GONPs and 50 wt.% GGBFS witnessed an increase in its flexural strength up to 58.5% during 28 days and 59.2% during 90 days. The results indicated that by adding 0.1 wt.% GO and 50 wt.%, concrete chloride permeability decreased substantially 72% for 90 day cured samples compared to OPC. GONPs as an alternative to cement up to 0.1% by weight can accelerate the formation of C-S-H gel, thereby increasing the strength and improving the resistance of water absorption and chloride permeability. The effects of pozolanic reaction in the concrete leading to the filling of the pores were significant factors in the proposed curtailment mechanism.*

Keywords: *Concrete, Durability, Graphene Oxide, Ground Granulated Blast Furnace Slag.*

1. INTRODUCTION

Concrete plays an important role in the development of the modern world and in the meantime, Ordinary Portland cement (OPC) is a main and integral material in the construction industry. [1, 2]. The production of each ton of cement consumes 1.5 tons of raw materials and emits 0.9 tons of CO_2 into the atmosphere. This is equivalent to 7% of the world's total carbon dioxide emissions [1, 3-6]. On the other hand, The industry consumes 60% of the raw materials in the lithosphere, which is equivalent to 32% of the world's resources. According to studies, the industry consumes 12% of the world's water and 40% of the world's energy resources. Also, one of the problems of concrete structures at the seaside is the penetration of chlorine ions in the corrosion of reinforced steel and the destruction of concrete [8, 9]. The use of industrial waste materials in the production of sustainable alternatives to cement use in concrete instead of cement is one of the effective methods to reduce the consumption of raw materials, reduce energy costs, a significant reduction in greenhouse gas emissions from cement production, increase the corrosion resistance of concrete and increasing the durability of concrete [7, 10]. Based on the above explanations, extensive studies have been conducted on the replacement of waste materials instead of cement (above 50%), which can be referred to the use of complementary cementitious materials such as blast furnace slag, fly ash (FA), silica fume, etc. Alternatives to cement such as ground granulated blast furnace slag (GGBFS) is used as a complementary cementitious alternative to cement for construction applications for enhanced properties and also maintaining environmental sustainability and reduce cost [5, 6]. Materials such as ground blast furnace slag, fly ash (FA), silica fume, etc. are added to concrete mix at more than 50% by weight to produce concrete with enhanced durability, corrosion resistance, mechanical at the same time reducing CO_2 emissions, raw materials and energy consumption thus, help with drive for sustainability in construction industry [5, 6]. Milled slag enhances the cement hydration process and general physico-chemical properties by affecting the final product's porosity and transport properties [3, 7]. Although cements containing 50 wt.% steel slag are shown to have

[DOI: 10.22068/ijmse.2725]

good binding performance [7] according to the conducted studies, GGBFS-added concretes are slow at gaining the maximum strength, but this can be counteracted by temperature and curing time [8-12] and those containing 40, 60, and 80 wt.%, exhibited enhanced mechanical and flexural strength with the 60 wt.% one having the maximum tensile and flexural strength [13]. Mo et al. [14] report a near 24% reduction in the 28-day compressive strength in the 60% samples, while Gsoglu et al. [15] showed an 11% in 90-day compressive strength of the same. Investigation of the strength, porosity, and chloride permeation characteristics of concretes containing high slag content 50 wt.% or more GGBFS indicated higher resistance to chlorides ion penetration [8]. Experiments on similarly composed concretes for up to 180 days showed significant reduction in the chloride ion diffusion [16-27]. In a longer duration experiment on electrical resistivity of two concrete mixes with 50% and 70% slag, Kayali et al. [28] report 35% and 24% reduction respectively in the Coulomb charge passed of concrete specimens at the age of 350 days. Yeau and Kim showed that the chloride ion diffusion coefficient of concrete samples decreased after 28 days with partial replacement of cement with 55% slag compared to ordinary concrete [21]. Similar results are reported from steel making slag fortified self-compacting concretes' mechanical and durability characteristics that are both environment-friendly and low cost [29]. A comprehensive study covering the, mineralogical, physico-chemical as well as mechanical effects on the concrete upon addition of slag showed a markedly improved strength and rheological properties [30]. As mentioned above, addition of slag is beneficial only within a percentage range. Gupta showed decreased water permeation in concrete containing 60% slag for 90-day cured samples [23]. Very long term follow up of the effect of slag admixed concretes on chloride penetration; one for 25 years [31] on two concrete mixes with 45% and 65% slag exposed to intermittent tide and the other for 50 and 100 years [32] both confirm the retarding effect of slag additions. Fraj et al. [33] investigated the ingress of chlorides during the hardening of slag-blended mortars that may have been exposed at the outset to chlorides and showed the slowing down of the hydration reaction and the filling of capillary pores. The gradual formation of the hydrates within the hardening microstructure obstructs the chloride diffusion paths, lowering the overall chloride diffusion coefficient which was measured as 12×10^{-12} m^2/s after 28 days of exposure is, for 0%, 14.2×10^{-12} m^2/s for 30% and 14×10^{-12} m^2/s for 60% slag mixed concretes. In a similar way, Duraman and Richardson [34] demonstrate that GGBFS lowers CH formation and porosity while the effect of slag on reducing super saturation of pore solutions with respect to CH and inhibiting the nucleation and growth of C–S–H is also shown [35]. Milled slag effect on reducing porosity has been observed [36, 37]. Sadawy and Nooman [38] report that concretes incorporating nano sized blast furnace slag results in a higher density and diminished XRD-peaks intensities from portlandite. Furthermore, such addition significantly enhanced the mechanical properties, durability and corrosion resistance. The combination of slag and as much as 2% silica fume causes improved strength and corrosion properties [39]. Fly ash has similar positive effect on the strength and the durability of concrete due to the higher pozzolanic activity which significantly increased the interfacial bond strength of the concrete [40]. This concrete exhibited good chloride penetration resistance due to reactions between the alkali activated slag and cement to form C-S-H (hydrated calcium silicate), and C-A-H (hydrated calcium aluminate) gels [41]. The admixture of around 1% nano-$CaCO_3$ improves compressive strengths and durability properties of slag blended concretes [1]. Nanomaterials have been used as additives to enhance strength and curtail chloride penetration in concretes. Concurrent addition of GGBFS and GO enhanced both compressive, tensile and flexural strength with improved resistance to chloride permeation [42-48]. In general, two mechanisms of nanomaterial additions i.e. seeding and nucleation and filler effect are presented to explain increase in the mechanical strength of cementitious composites the first postulates that the large surface area specific to the nanomaterials provides numerous nucleation sites for hydration process while the latter helps with filling the pores inside the concrete matrix [49]. The effects of GO on the microstructure and mechanical properties of cement-based concrete at the micro level has been published leading to a denser microstructure by reducing the total pore

[DOI: 10.22068/ijmse.2725]

volume of the cementitious composite [50-55]. However, despite proven acceleration in hydration process its effect on the C-S-H, formation is not conclusively shown. The faster hydration by addition as little as 0.05-0.2 wt.% GO as demonstrated by work of Jing et al. [56] leads to enhanced mechanical properties including up to nearly 80% increase in tensile strength, 40% improved compressive strength with variable results in reported [57-62]. GO could help improve the basic properties for the cement-based by altering the microstructure of cement hydration products and refining the crystal size, to form a dense less porous and uniform structure. This will retard crack initiation and growth [62-65]. GO addition has also been shown to decrease formation of large capillary pores thus impeding diffusion of chloride [66]. Promising trends indicative of prolonging of service life of concretes containing G, GO, and GGBS are published [67]. One of the main problems encountered when admixing G or GO nano particulates is their satisfactory dispersion. Improved GO dispersion was observed by adding silica fume or fly ash to the cement paste [68-70]. GO has found increased use in place of the various single and multi-walled CNT and CNFs in different fields since it is cheaper sometimes by a factor of 1000 times [71]. Nowadays, under different environmental conditions, structures do not function as expected. Damages in the form of structural cracks caused by stress as well as scaling and shrinkage caused by loss of fine aggregates and high wear, leakage, etc. lead to the failure of concrete structures. In addition, use of ordinary concrete leads to premature destruction of structures. Therefore, use of high-strength concrete containing GGBFS and GO as a building material in marine structures can be useful. Using such high-performance concretes can reduce the cost of materials by reducing the thickness of the structure, increasing the mechanical, physical and corrosion properties, and saving the required materials.

No study has been reported on GO and GGBFS inclusion in concrete composites with regards to durability and chloride permeation to get a clear picture of whether or not this investigation will be helpful for practical application in construction industry. To this end, this study was carried out to develop a Nano-reinforced concrete composite with addition of GO and GGBFS. The present study put the main focus on the application of GO-GGBFS as a Nano-filler in developing a concrete for industrial applications in marine environment. In this paper, durability and the chloride ion penetration into the ordinary concrete and that containing GO and GGBFS under different conditions was measured.

2. EXPERIMENTAL PROCEDURES

Ordinary Portland cement (OPC) according to ASTM C150 [72] standard was used. The chemical composition of the cement are shown in Table 1. The microstructural and analytical studies such as Field emission scanning electron microscopy (FE-SEM), X-Ray Diffraction (XRD), energy-dispersive X-ray spectroscopy (EDS), X-ray fluorescence (XRF) and Fourier transform infrared spectroscopy (FTIR) were performed on the materials or concrete samples. The nanoparticle size distribution pattern of the used OPC has been shown in Fig. 1.

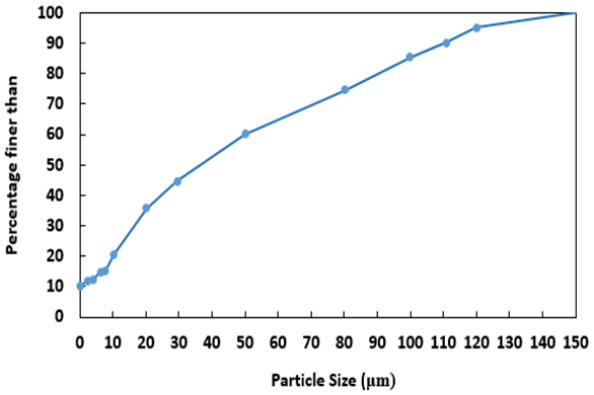

Fig. 1. Particles distribution pattern of ordinary Portland cement

The GGBFS was procured from local sources with Blaine fineness of 3500 cm^2g^{-1}. The CaO/SiO_2 ratio was 1.4 based on XRF analysis (Table 1).

Fig. 2 shows the FTIR spectroscopy results of GONPs used in this study from Hummer method. As observed, Graphene oxide has different functional groups including hydroxyl, epoxy, carboxyl, phenol, ether, and aldehyde. The strong vibration band in the region of 3399.77 cm^{-1} is attributed to the OH hydroxyl group resulting from moisture absorption. The tensile vibration bands in 1727.69 cm^{-1} and 1620.71 cm^{-1} are related to carbonyl bonds C=O and bond C=C, respectively.

[DOI: 10.22068/ijmse.2725]

Table 1. Chemical analysis of Portland cement and GGBFS (wt.%)

Material	Supplier	SiO_2	Al_2O_3	Fe_2O_3	CaO	MgO	Na_2O	K_2O
Cement	Tehran Cement Company	21	4.50	4	65.6	2.3	0.25	0.41
GGBFS	Boton Sabz Company	31.10	9.16	1.17	43.64	6.17	0.55	1.11

While the tensile vibration in 1364.36 cm^{-1} band belong to C-OH bond, 1226.86 cm^{-1} and 1064.76 cm^{-1} belong to CO bond of epoxy group.

The vibration band of 515.51 cm^{-1} indicates CH bond. Peak intensities confirm the presence of these functional groups as the main groups in graphene Nano-oxide after the oxidation process, which is consistent with the findings from the published literature [73].

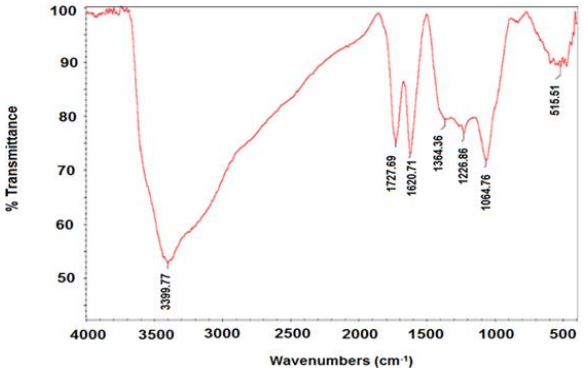

Fig. 2. FTIR graph of GO produced by Hummer method

The XRD diagram of graphene Nano-oxide used in this study is shown in Fig. 3. Based on the obtained diffraction spectrum, all peaks related to primary graphite are removed, and the only peak observed in the XRD spectrum is related to graphene oxide Nano-plates which is in agreement with the results from the literature [74, 75]. The singular peak shown at the scattering angle of 2θ= 12° corresponds to the (001) graphene oxide plate, and lack of any other peak is indicative of complete graphite oxidation and high purity of graphene oxide. The results confirmed that oxygenated functional groups were introduced between the primary graphite plates, thus weakening the interactions among them. This helps the graphene oxide sheets disperse more easily as stable suspension. The plate spacing in the graphite structure is 2.9 to 3.6 angstroms and in the case of graphene oxide, it is about 7 angstroms, which is indicative of an increase in the distance between the primary graphite plates in the process of producing graphene oxide, thus confirming the entry of functional groups between the graphene oxide plates [74, 76].

The FE-SEM microstructure images of GO nanoplatelets used in this study are shown in Fig. 4, according to which the particle length varies from 2 µm to 15µm and the average thickness is 7.7 nm. The FE-SEM images show the morphology of graphene oxide nanosheets to be wrinkled thin lamellar layers interlinked to form a three-dimensional porous structure. The inter-planar distance in the crystalline GO structure could be calculated from XRD pattern using Bragg's law: λ= 2dsin(θ), where λ is the X-ray beam wavelength (in this case λ=1.54 A°), d is the distance between adjacent layers, Θ the diffraction angle. According to XRD analysis in Fig. 3 and microstructure images in Fig.4, d= λ/2 sin (θ)= 1.54 A°/2sin(θ) which for the initial sharp peak would come to 6.8 Å. The elemental analysis and physical properties of the GO are shown in Fig. 5 and Table 2.

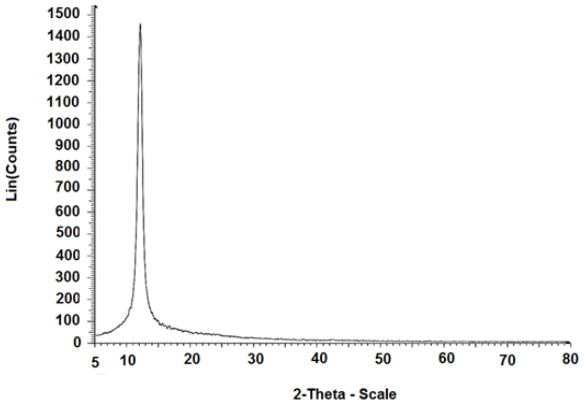

Fig. 3. XRD analysis of dry GO before dispersion in water

Concrete mixes with compositions shown in Table 3. Polycarboxylate was used as a super plasticizer and 0.5% by weight of cement in all samples. GGBFS was used as a replacement of Portland cement and GONPs added to concrete as an additive.

[DOI: 10.22068/ijmse.2725]

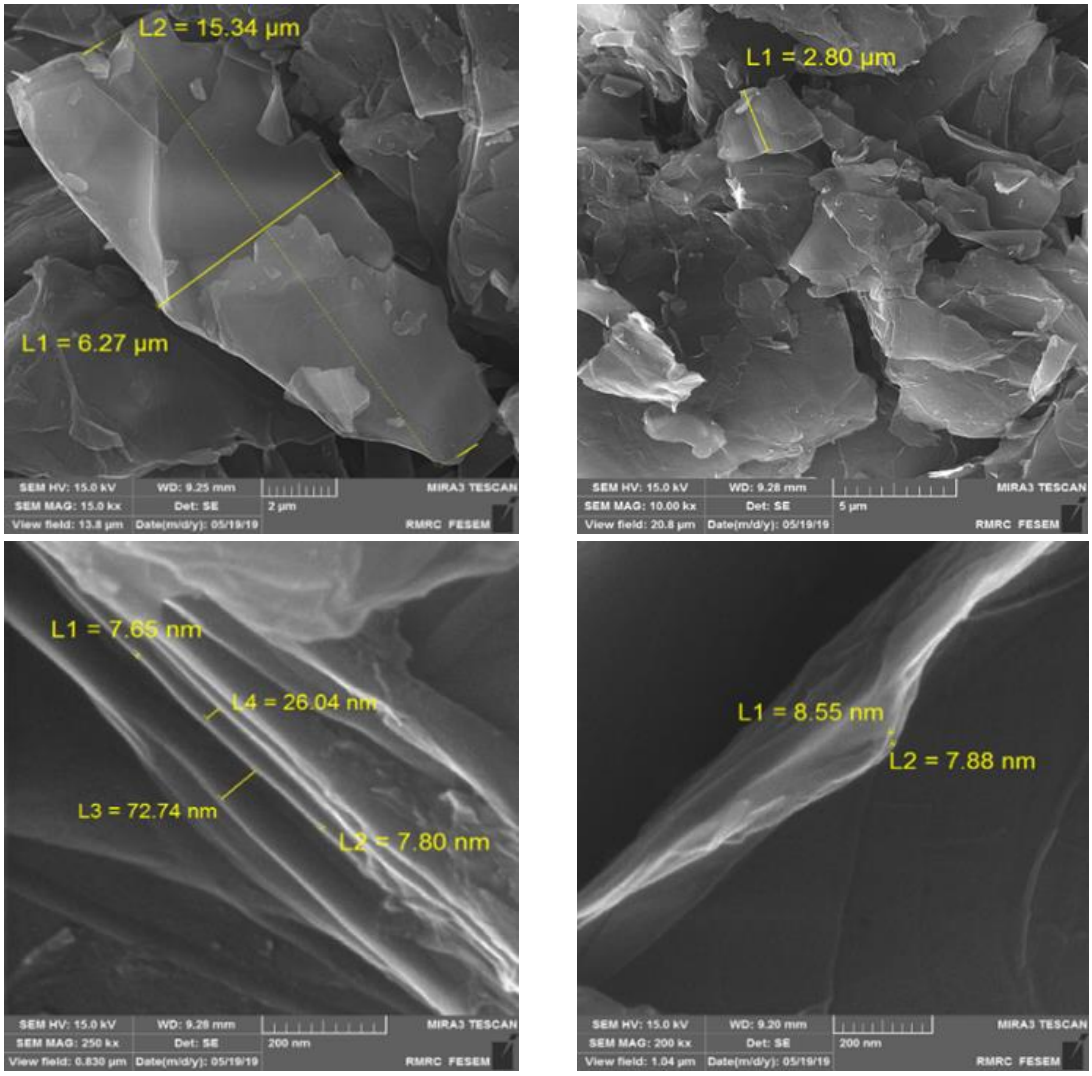

Fig. 4. FE-SEM images of graphene oxide Nano sheets

Table 2. Physical properties of commercially procured GONPs

Supplier	Original Packaged Form	No. of Layers	Platelet Thickness (nm)	Size (µm)	Purity (%)
India Tech Company	Black powder	5-8	7.5-8.5	2-16	> 99

Table 3. Quantity of materials used in m^3 of Concrete Samples

Series	MIX	GGBFS (wt.%)	GO (wt.%)	GGBFS (Kg/m^3)	GO (Kg/m^3)	OPC (kg/m^3)	Water (kg/m^3)	FA (kg/m^3)	CA (kg/m^3)	SP (kg/m^3)
GGBFS	OPC	0	0	0	0.0000	425	170	1005.5	676.5	0.0425
	S30	30	0	127.5	0.0000	297.5	170	1005.5	676.5	0.0425
	S40	40	0	170	0.0000	255	170	1005.5	676.5	0.0425
	S50	50	0	212.5	0.0000	212.5	170	1005.5	676.5	0.0425
	S60	60	0	255	0.0000	170	170	1005.5	676.5	0.0425
GO-GGBFS	S50-GO0.01	50	0.01	212.5	0.0425	212.5	170	1005.5	676.5	0.0425
	S50-GO0.05	50	0.05	212.5	0.2125	212.5	170	1005.5	676.5	0.0425
	S50-GO0.1	50	0.1	212.5	0.425	212.5	170	1005.5	676.5	0.0425
	S50-GO0.2	50	0.2	212.5	0.85	212.5	170	1005.5	676.5	0.0425

[DOI: 10.22068/ijmse.2725]

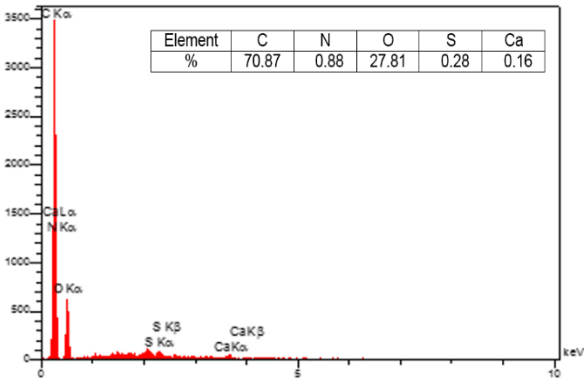

Fig. 5. Energy-dispersive X-ray spectroscopy (EDS) area elemental analysis of GO

Totally, two series of mixtures were prepared in the laboratory trials. GGBFS series mixtures were prepared by cement and 0%, 30%, 40%, 50% and 60% by weight of GGBFS replaced by Portland cement and GGBFS-GO series were prepared with different contents of GO Nano platelets.

The mixtures were prepared with the cement replacement by GO Nano platelets with 0.01%, 0.05%, 0.1% and 0.2%. The binder content of all mixtures was 425 kg/m^3. The mixing was carried out at the room pressure. The water to cement ratio (W/C) was kept at 0.4 throughout. The total dispersion of the graphene oxide is achieved through sonication using a 300W and 20 kHz frequency transducer for 30 minutes (Fig. 6). The graphene oxide and cement and aggregates mortar were mixed in a shear mixer for 3 minutes followed by 30 seconds on a shaker. The W/C ratio was kept constant by adding just the difference between the total water required and the water used to make the GO solution. Samples were made according to ASTM C192M-16 [77]. The samples were kept in the mold in the laboratory for 24 hours and placed in a bath containing lime for 28 and 90 days at 25°C and a relative humidity of 95%.

Several types of tests were carried out on the prepared specimens. ASTM C39 [78] and ASTM C293 [79] standard tests were respectively carried out to examine the compression and flexural strength of concrete specimens.

Split tensile tests were done in accordance o the ASTM C496 standard [80]. Rapid chloride permeability test (RCPT) was performed per ASTM C1202 standard test [81].

The total coulombs of electricity thus passed, would be proportional to the electrical resistance of the specimen which, inversely relates to chloride ion penetrating the sample. So, the lower the electric current passed indicates higher resistance to chloride ingress. For determining the resistivity of concrete, Resistivity test was applied with modifications based on AASTHO TP 95-11 standard [82, 83] using a Wenner array probe. Water absorption values of concrete samples were measured as per ASTM C642 standard [84] after 28 and 90 days of curing. Conduction calorimetry test was performed in accordance o the ASTM C1679-08 standard [85] at 22°C for a maximum of 70 h. Total porosity and pore size distribution were determined using mercury porosity (Mercury Intrusion Porosimetry-MIP) based on ASTM D4404 standard [86] with a maximum pressure of 200 MPa. A contact angle of 130 degrees and pores between 10 and 1000 nm were selected.

Thermogravimetric analysis (TGA) and differential thermogravimetric (DTG) analysis were performed on the samples as per ASTM C1872-18 standard [87]. Specimens which were cured for 28 days were heated from 105 to 1000°C, at a heating rate of 10 °C/min and in an inert N_2 atmosphere.

Fig. 6. Sonication devise used to form the GO mix

[DOI: 10.22068/ijmse.2725]

In order to perform the electrochemical impedance spectroscopy (EIS) tests, specimens were prepared. To make concrete specimens, steel reinforcement was placed in the center of the fabricated cylinder mold. Before placing the steel reinforcement in the concrete sample, a height of 6 cm was selected as the test surface and the rest of the reinforcement was sealed with epoxy primer and Teflon tape on it to prevent the penetration of chlorine ions and damage the reinforcement. Fig. 7 shows a concrete sample prepared for the EIS test and test set up.
All specimens were immersed in a 3.5% brine (NaCl) solution for 3 day before test. Silver chloride electrode (Ag/AgCl) was used as a reference electrode and a 304 stainless steel sheet in a semicircle around the concrete sample was used as an auxiliary electrode. The frequency of the test was considered from 1-10 MH and the voltage range was 10 mV. The corrosion test results were evaluated by Z-View software.

3. RESULTS AND DISCUSSION

Table 4 shows the physical structure characteristics of concrete specimens. Table 4 shows that in GGBFS specimens with increasing GGBFS content, the total volume of specific pores of concrete decreases and the diameter of concrete pores decreases. This decrease in porosity is attributed to the addition of GGBFS, which caused the samples to condense. According to the results of Table 4, after the addition of GO and GGBFS, the structural porosity of concrete is significantly reduced and a denser structure is created.
The effects of pozzolanic reaction in concrete fill the pores and cracks and due to the filling of pores and cracks, the concrete is compacted and its resistance to chloride ion penetration is improved [88]. When GGBFS is added to the cement mixture, the hydrated calcium silicate is formed instead by the direct interaction of calcium hydroxide and GGBFS [92-93].

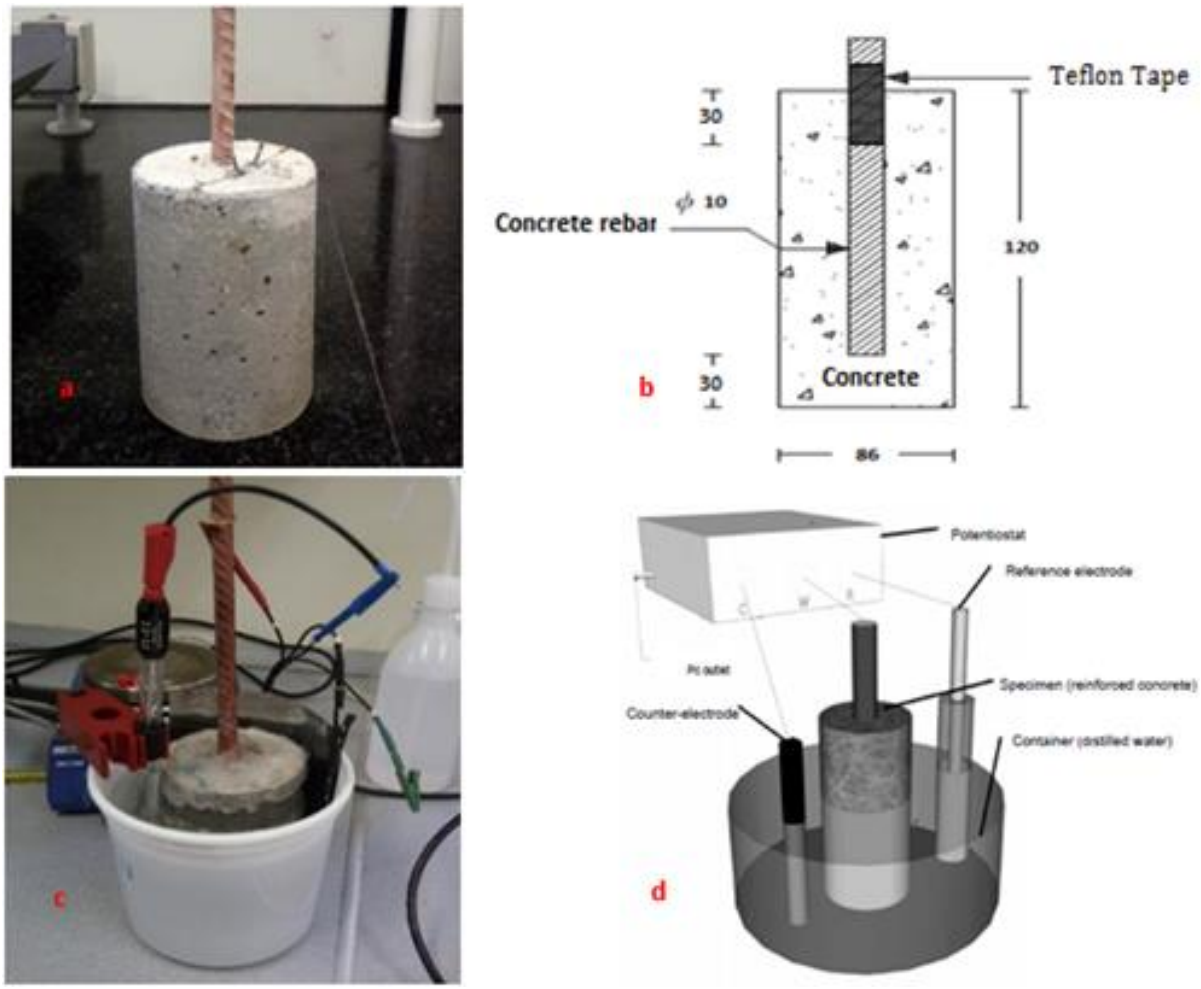

Fig. 7. Concrete sample prepared for EIS (a, b) and test set up for EIS (c, d)

[DOI: 10.22068/ijmse.2725]

This is a good adhesive and results in improved mechanical and physical properties. Anhydrous cement is composed of four types of minerals namely alite (C_3S), belite (C_2S), aluminate (C_3A) and ferrite (C_4AF). Upon adding water to cement grains, various chemical reactions occur simultaneously to give rise to the formation of a rigid cement paste. The resulting porous multi-phase matrix contains CH with traces of aluminates and unhydrated clinker embedded into the binding agent, C–S–H gel. The CH by-product is responsible for the cement alkalinity. Thus, extra attention should be paid towards dispersing nanomaterials in a high pH value cement medium. Moreover, the heterogeneous nature of cement contains mostly calcium ions with traces of magnesium, aluminum, iron, potassium, sodium and sulfur ions. The interaction of nanomaterials Table 5 shows the calorimetric conductivity of GGBFS samples. One peak corresponds to the production of C-S-H and CH gels, and the other peak to the conversion from ettringite (AFt) to the calcium monosulfo-aluminate (AFm) phase through dissolution and reaction with $Al(OH)^{4-}$. The heat rate values in Table 5 show that increasing the percentage of GGBFS in the pastes accelerates the peak time. The total heat released decreased with increasing GGBFS. The presence of GGBFS in concrete reduces its heat of hydration. According to the results shown in Table 5, increasing the percentage of GO nanoparticles up to 0.1 wt.% reduced the peak times and heat rates. It is noteworthy that GO functional groups play a very important role in this phenomenon [57, 94].

Fig. 8 shows the TGA and DTG results of the GGBFS and GO-GGBFS samples measured in the 110-1000°C range. The results show that after 28 days of curing, the weight loss of the samples increases with increasing GGBFS content in concrete (Fig. 8(a) and Table 5).

Table 4. Properties of the pores in GGBFS and GO-GGBFS specimens

Sample	Total Specific Pore Volume (mL/g)	Most Probable Pore Diameter (nm)	Porosity (%)	Average Diameter (nm)	Pore size Distribution (mL/g)		
					Pores (10-50 nm)	Pores (50-200 nm)	Pores (>200 nm)
OPC	0.0341	17	9.12	11.4	0.0061	0.0114	0.0039
S30	0.0308	15	7.00	9.6	0.0069	0.0093	0.0032
S40	0.0279	13	6.86	9.2	0.0078	0.0089	0.0030
S50	0.0263	11	6.69	8.4	0.0089	0.0081	0.0027
S60	0.0276	12	6.79	8.7	0.0081	0.0085	0.0029
S50-GO0.01	0.0235	11	6.00	7.3	0.0089	0.0071	0.0026
S50-GO0.05	0.0223	9.7	5.87	6.8	0.0093	0.0066	0.0024
S50-GO0.1	0.0211	9.1	5.78	6.2	0.0096	0.0061	0.0021
S50-GO0.2	0.0220	10.2	5.86	6.5	0.0092	0.0063	0.0022

Table 5. Calorimetric results and weight loss (%) of the pastes in the range of 105–1000°C at 90 days of curing of C0-GGBFS and N-GGBFS specimens.

Sample	Total Heat (Kj/Kg)	First Peak		Second Peak		Total Weight Loss in the Range of 105-1000oC (%)
		Time (h)	Rate (W/kg)	Time (h)	Rate (W/kg)	
OPC	412.3	3.6	0.98	29.3	5.51	11.45
S30	398.5	3.3	0.95	27.3	5.40	11.93
S40	380.1	3.1	0.89	26.8	5.37	12.09
S50	363.4	2.9	0.79	26.1	5.21	12.33
S60	370.7	3.1	0.86	26.0	5.32	12.67
S50-GO0.01	365.2	2.7	0.89	25.7	5.23	12.82
S50-GO0.05	368.1	2.4	0.91	25.2	5.28	12.98
S50-GO0.1	373.1	2.1	0.95	25.0	5.37	13.64
S50-GO0.2	369.4	2.2	0.93	25.1	5.31	14.43

[DOI: 10.22068/ijmse.2725]

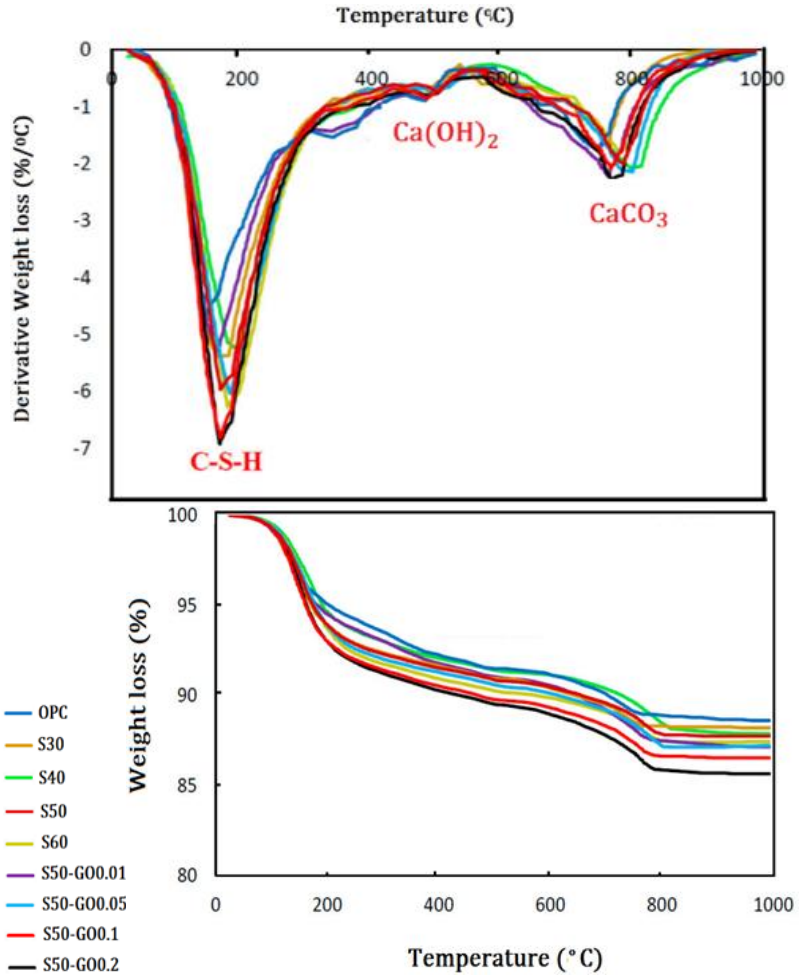

Fig. 8. (a) Thermogravimetric analysis (TGA) and (b) differential thermogravimetric (DTG) analysis in GGBFS and GO-GGBFS specimens

Also it can be seen, with increasing GO nanoparticles in concrete up to 0.1% by weight, the weight loss changes of the samples have increased. Generally, GO accelerates the rate of hydration by providing preferential nucleation site at its oxygen functional groups [57]. As shown in Fig. 8(a) and (b), three significant decomposition stages can be found in the curves, i.e. 105–400°C, 400–600°C and 600–800°C. The first peak can be assigned to the evaporation of free water (before 105°C) and the decomposition of ettringite (110–170°C), carboaluminate hydrates and C-S-H (105–400°C) [95, 96]. The second peak is related to the decomposition of portlandite while the third peak is related to the decomposition of calcium carbonates [95, 97].

The functional groups of GO plays a major role as the growth points of hydration products by attracting C_3S, C_2S and C_3A. GO addition does In general, the addition of GONPs improve the structure of concrete pores. GONPs has several not change the types of hydration crystals, but only promotes the formation of hydration productions. The hydration crystals closely interweave with each other and form a compact microstructure. Obtained results suggest the oxygen functional groups of GO could act as nucleation sites for crystals, which subsequently reinforces the generation of hydrated productions. Furthermore, the amount of functionalized oxygen groups has significant influences on the hydration and mechanical strength of hardened cement paste. More oxygen groups lead to higher hydration degree and more productions, which contributes to the improvement in mechanical and physical properties.

This research provides an in-depth understanding of the role of oxygen functional groups in the formulation of GO modified cement composites [94].

[DOI: 10.22068/ijmse.2725]

important roles in this process, including [49, 98]:

1. GONPs as a filler increases the density of concrete and this phenomenon leads to a significant reduction in the porosity of concrete.
2. GONPs as an activator accelerates the hydration of cement.
3. GONPs acts as a nucleus in the cement paste, which reduces the size of the $Ca(OH)_2$ crystal and makes tropism more random.

Fig. 9 shows the XRD results of the GGBFS and GO-GGBFS samples. The enhancement in the formation of hydrated products can also be seen in Fig. 9 that shows the XRD results of the GGBFS and GGBFS-GO samples. The three main hydration peaks (A, D, E) are much more pronounced for S50-GO0.1 compared with either PC or any other composition tested. According to Fig.s 8 and 9 GONPs played important role in the formation of $Ca(OH)_2$ and C-S-H gels at early ages of cement hydration.

Fig. 10 depicts the SEM images of OPC, S50 and S50- 0.1GO samples after 28 and 90-day curing time. As can be clearly seen obviously, after replacement of GGBFS, the structural porosity of the concrete was significantly reduced, hence a dense structure. Beneficial effects of GGBFS on concrete are due to the modified microstructure of the cement paste, which has more capillary pores filled with C-S-H gel with a lower density than the Portland cement paste [95-104]. Fig. 10 shows the areas with folded plate morphology of graphene oxide sheets and a more compact mixture after all days of curing which indicate rapid formation of C–S–H gel in presence of GO nanoparticles. As shown before, both milled slag and GO modify microstructure by filling the pores with lower density C-S-H gel and speeding up the process of hydration and crystal nucleation. Although powdered slag on its own can effectively reduce the pore size through acting as nucleation sites its chemical reactivity in calcium hydroxide environment to form C-S-H gel and its movement through capillary passages leads to a dense microstructure.

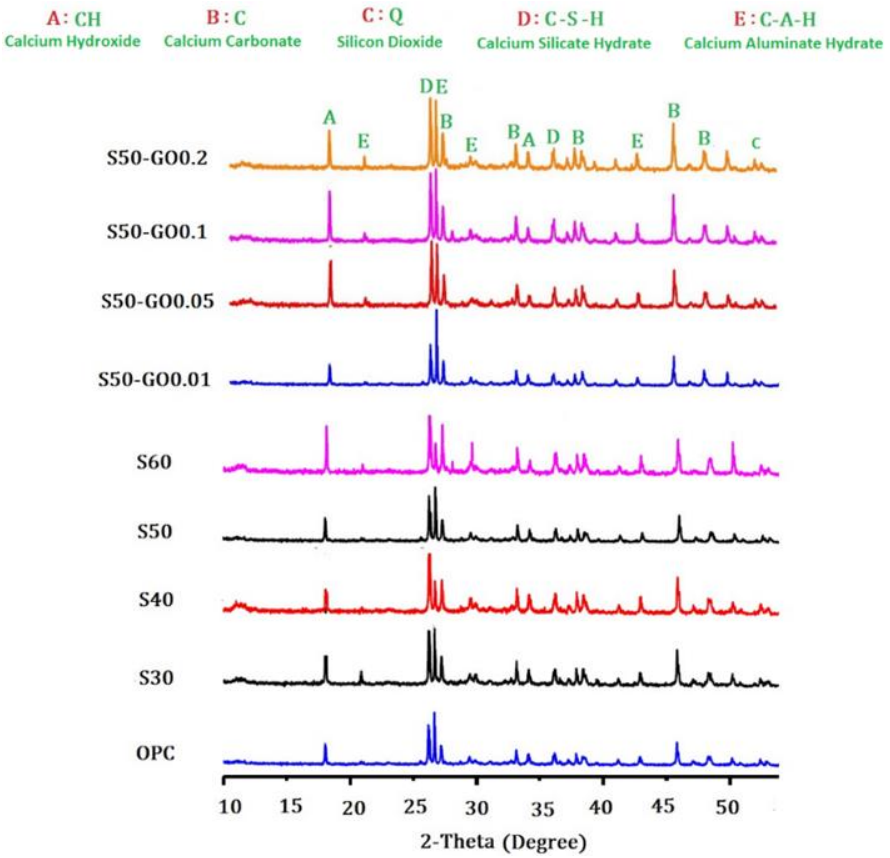

Fig. 9. XRD results indicating the formation of hydrated products for different GGBFS and GO-GGBFS specimens

[DOI: 10.22068/ijmse.2725]

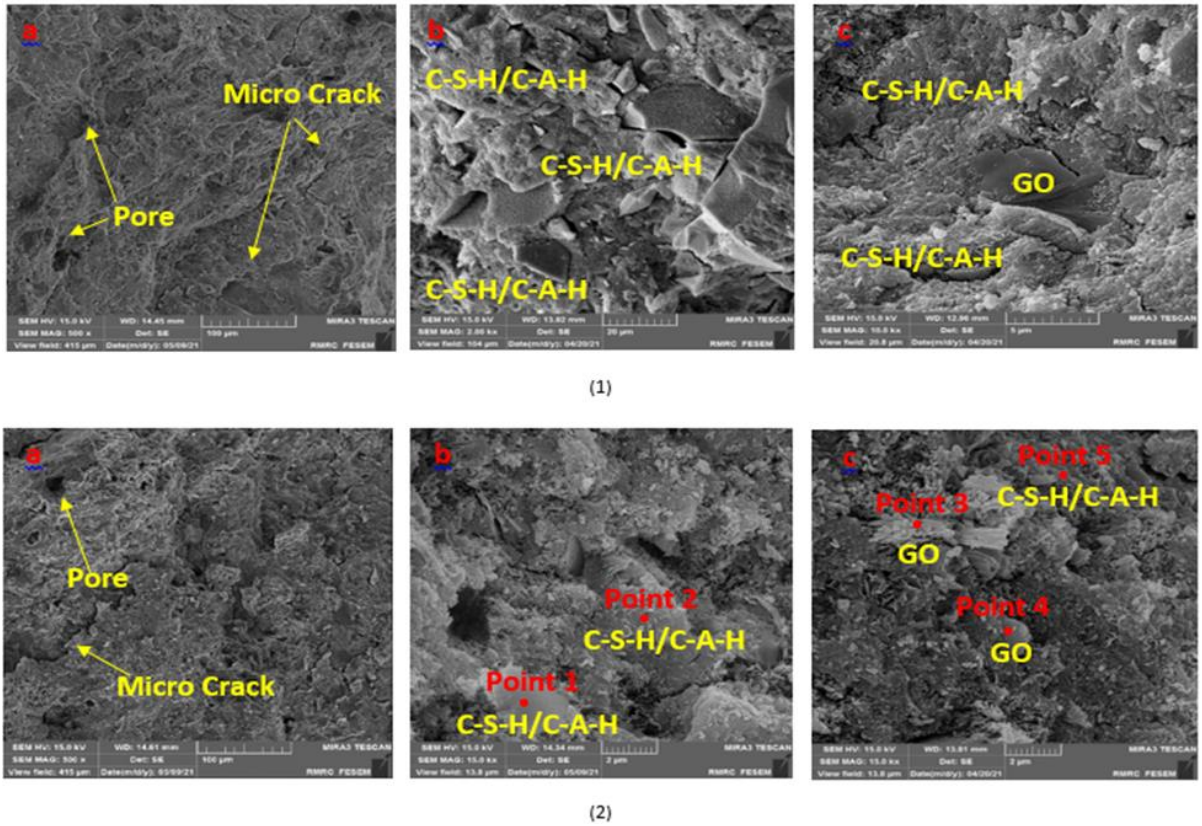

Fig. 10. SEM micrographs of (a) OPC specimen, (b) S50 specimen, (c) S50- 0.1GO specimen and at 28 days (series 1) and 90 days (series 2) of curing

In order to investigate the composition–microstructure relationship for the GO–cement composites, energy-dispersive X-ray spectroscopy (EDS) was employed to analyze the 5 points marked in Fig. 10 and results are shown in Table 6. It should be noted that element H cannot be detected by EDS due to its very low atomic weight. C–S–H gel is essentially composed of Ca, Si, and O, with a small amount of Al, S, and Fe, indicating that the C–S–H gel interwove with AFt/AFm and C–H at 90 days. After the addition of GO, a large percentage of element C and a considerable increase in element O were observed in C–S–H for Points 3 and 4. It is noticed that a small amount of element C was also found in C–S–H for Point 5. This may be due to the fact that the GO absorbed a large amount of water molecules and ions and became the nucleation sites of hydration products, which in return regulated and refined the formation of hydrated crystals.

Fig. 11(a) show the compressive strength of GGBFS specimens after 28 and 90 days of curing which are all increased by increasing GGBFS up to 50%. Fig. 11(a) also show the compressive strength of GO-GGBFS specimens at 28 and 90 days of curing. The results show that the compressive strength increases by adding GO nanoparticles up to 0.1 wt.% replacements and then it decreases. As mentioned above, the hydrated calcium silicate is formed instead by the direct interaction of calcium hydroxide and GGBFS.

Table 6. Major element composition of the sample points in Fig. 10

Point No.	Element Weight Percentage (wt. %)						
	O	Al	Si	S	Ca	Fe	C
Point 1	45.43	5.87	2.75	10.2	35.33	0.42	-
Point 2	21.65	2.45	14.23	1.11	58.28	2.28	-
Point 3	35.58	3.12	10.58	-	17.84	-	32.88
Point 4	37.03	3.75	11.12	-	16.54	-	31.56
Point 5	27.71	2.13	17.14	0.61	46.71	1.09	4.61

[DOI: 10.22068/ijmse.2725]

This is a good adhesive and results in improved mechanical properties. Using more than 50% GGBFS has reduced the compressive strength of the specimens. It may be as a result of the reduced CaO content in GGBFS in comparison with Portland cement. This may reduce the amount of crystalline $Ca(OH)_2$ and hence C–S–H gel. The functional groups of GO plays a major role as the growth points of hydration products. The amount of functionalized oxygen groups has significant influences on the hydration and mechanical strength of hardened cement paste. More oxygen groups lead to higher hydration degree and more productions, which contributes to the improvement in compressive strength. The reduced compressive strength by adding more than 0.1 wt.% GO nanoparticles may be due to this fact that the higher the amount of graphene oxide in the cement field, the greater the possibility of agglomeration of the particles and therefore their homogeneous distribution in all cement fields will be difficult [105, 106].

Fig. 11(b) and Fig 11(c) also show the flexural strength and the split tensile strength of GGBFS and GO-GGBFS series concretes. Similar to the compressive strength, the flexural strength and the split tensile strength of all GO-GGBFS specimens is more than those of GGBFS specimens.

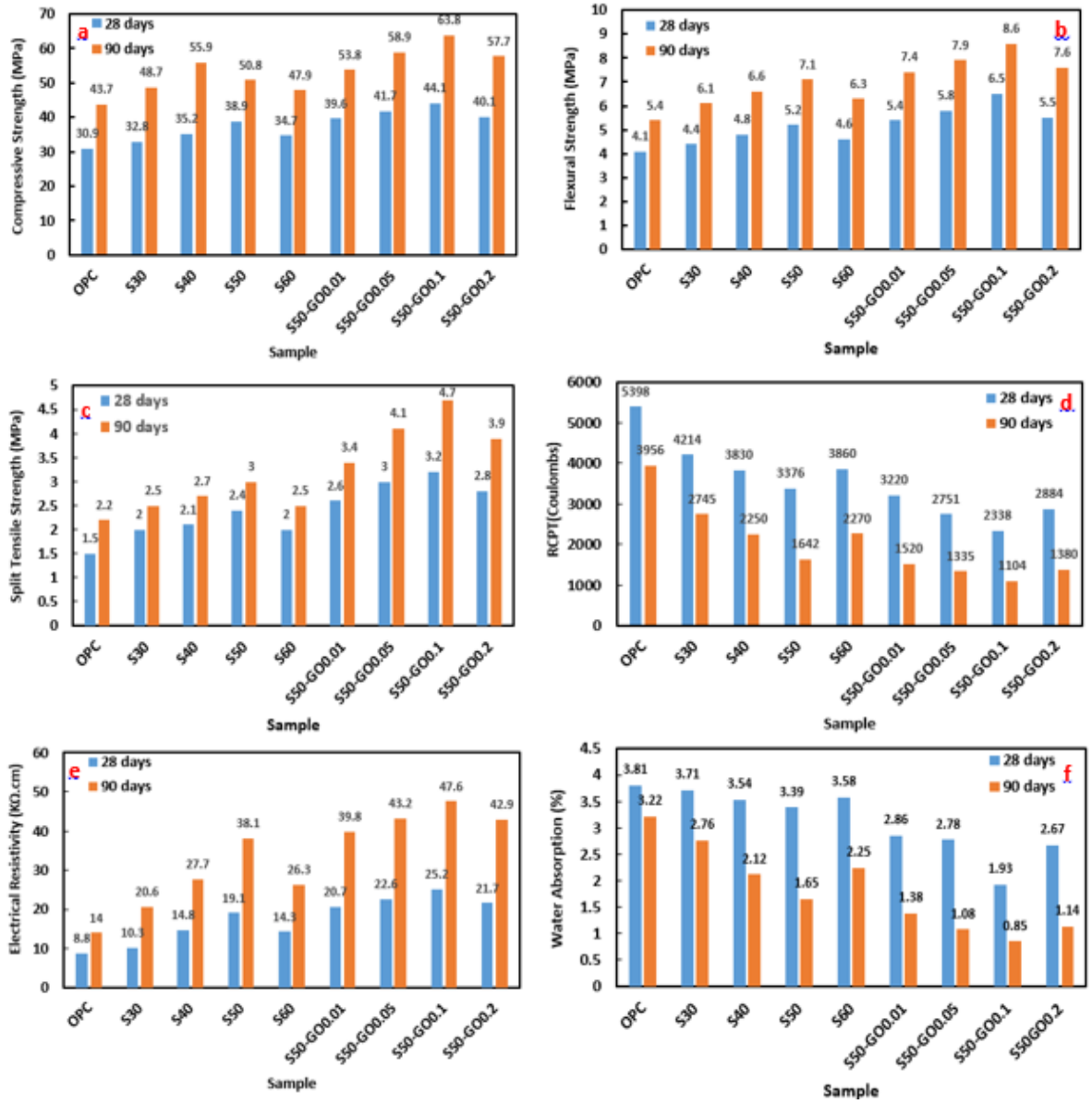

Fig. 11. Mechanical and physical tests results of concrete samples at curing time 28-days and 90-days

[DOI: 10.22068/ijmse.2725]

In addition, the flexural strength and the split tensile strength of GO-GGBFS series is increased by adding GO nanoparticles up to 0.1 wt.% and then it is decreased, similar to the compressive strength results. Fig. 11(d) and Fig. 11(e) show Wenner test and RCPT results for 28 and 90-days cured samples respectively. The observation that the addition of GGBFS in 28 and 90 days cured samples significantly decreases the charge conducted in RCPT tests signifies the increased resistance against chloride penetration. Free chloride is known for fast diffusion into concrete, but GGBFS in concrete may reduce this by concrete's chloride binding capacity [107-109]. The ASTM 1202-12 Standard designates such charge conduction as low chloride permeability (Table 7) [81]. The addition of 0.1 wt.% GO could effectively reduce the passing current in the conductivity test and enhance the resistance of concrete to chloride penetration. The highest electrical resistivity was achieved (47.6 kΩ.cm) for 90-days cured S50-GO0.1 sample. Overall, GO in GGBFS concrete, has great impact on chloride permeability. Fig. 11(f) show the water absorption percentages in the GGBFS and GO-GGBFS series at 28 and 90 curing time. The results show that the percentage of water absorption in GGBFS and GO-GGBFS decreased with increasing GGBFS and GO nanoparticles. Therefore, it can be seen that with long-term curing, increasing the age and percentage of GO nanoparticles can lead to a reduction in permeable pores. This is due to the performance and high filler effects of GGBFS and GO nanoparticles.

Fig. 12 shows the results obtained from the EIS tests for OPC and S50-GO0.1 samples. Increasing the radius of the Nyquist semicircle in modified concrete can be considered as reducing the structural porosity inside the concrete (Fig. 12(a)) [110]. It can be concluded that the behavior of S50-GO0.1 sample is somewhat closer to the capacitive behavior (Fig. 12(b)). Bode plots were also drawn (Fig. 12(c)). This indicates a deviation of the system from the ideal capacitive behavior.

Table 7. Chloride ion penetrability based on charge passed according to ASTM 1202-12 Standard [81]

The charge passed (C)	Chloride ion permeability
>4000	High
2000-4000	Moderate
1000-2000	Low
100-1000	Very low
<100	Negligible

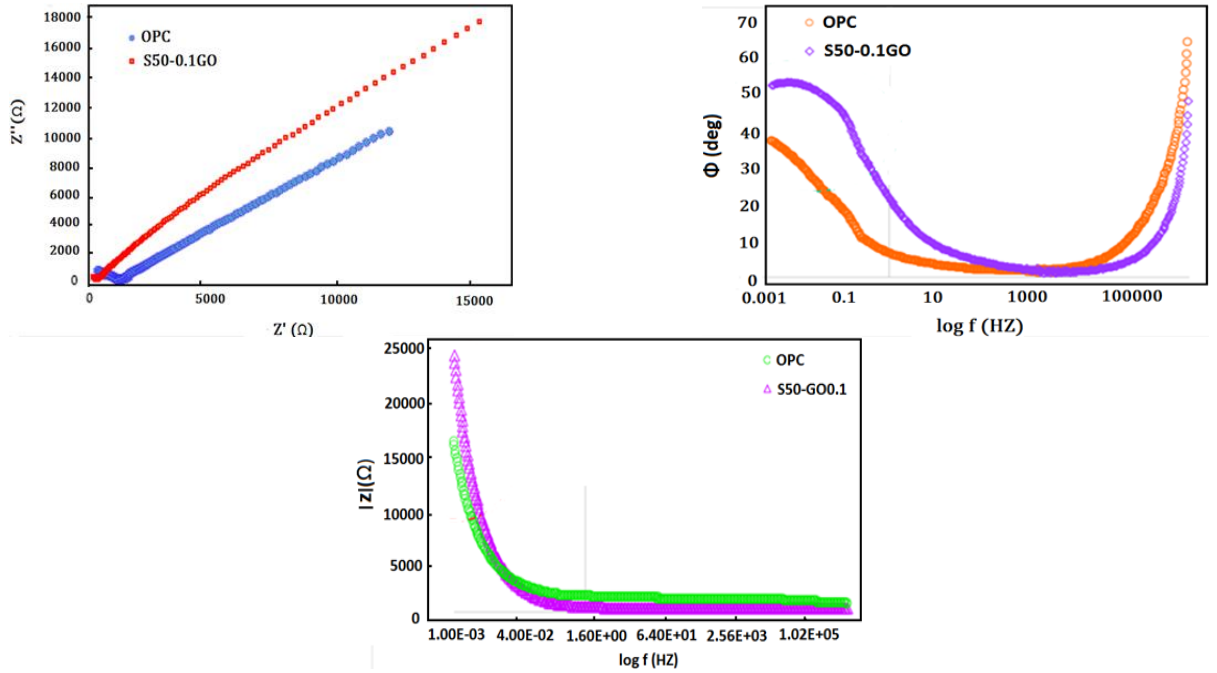

Fig. 12. AC impedance diagrams: a) Nyquist curves b) Bode-phase plots c) Bod plots of OPC and S50-GO0.1 samples after 90 days

[DOI: 10.22068/ijmse.2725]

The data obtained from the impedance test were entered and analyzed in Z-view software. The best circuit justified the experimental data. This circuit is shown in Fig. 13. In this circuit, Rp is the polarization resistance of the reinforcement, Rs is the ohmic resistance in the electrolyte, Rcon is the structural resistance of concrete which is related to its porous structure and CPEdl and CPEcon are values of the constant phase element relative to reinforcement and concrete respectively. The electrochemical values according to the selected circuit were obtained (Table 8). The results clearly show that the corrosion resistance of 0.1 Wt.% GO and 50 Wt.% GGBFS concrete is higher than that of OPC concrete.

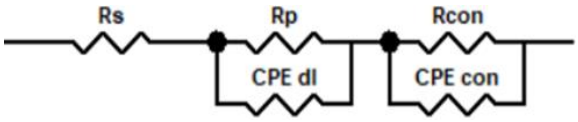

Fig. 13. The equivalent circuit used to simulate the experimental data

The cost of casting the mixed designed were analyzed and reported in Tables 9 and 10. The cost of concrete composites was evaluated using the commercialized market prices of the materials. The economic Index for strength (compressive strength/cost per m^3 of concrete) was observed to have maximum value at the mix S50-GO0.1 (with 0.1% GO inclusion) compare to rest of the mixes and The economic Index for Rapid chloride permeability (Rapid chloride permeability/cost per m^3) shows that the mix S50-GO0.1 is a better mix than the rest in terms of strength, chlorine ion permeability and economy.

Table 10 shows that the cost of materials for making S50-GO0.1 sample is 23% higher than this cost for OPC, but considering economic Index for Rapid chloride permeability, using this mix is cost-effective. According to this table, the economic Index for strength of S50-GO0.1 has increased more than 1.17 times compared to OPC and the economic Index for the rapid chloride permeability of S50-GO0.1 has decreased more than 4.46 times compared to OPC.

4. CONCLUSIONS

Throughout this study, the following concluding remarks were made:

- Incorporating GGBFS up to 50% by weight into the concrete improves its mechanical properties and the durability by producing a dense structure higher than OPC sample. It has been argued that utilizing GGBFS content more than 50 wt.% reduces the amount of CaO which is required for $Ca(OH)_2$ and subsequent C–S–H gel.
- Prolonging the curing duration in concrete samples with GONPs and GGBFS is essential to achieving higher levels of mechanical and physical properties.
- As the content of GO nanoparticles is increased up to 0.1 wt.%, the compressive strength, split tensile strength and flexural strength of the specimens is increased. This is due to more formation of hydrated products in presence of GO nanoparticles.
- Addition of 0.1 wt.% GO and 50 wt.% GGBFS would increase the mechanical strength of the concrete sample compared to OPC.

Table 8. Electrochemical impedance spectroscopy data calculated with Z-view software

Sample Code	Rp (Ω)	CPEdl-T (F)	CPEdl-P (n)	Rcon (Ω)	CPEcon-T (F)	CPEcon-P (n)
OPC	1119	1.15 × 10 -9	0.90	66550	0.0013	0.56
S50-GO0.1	280	2.90 × 10 -9	0.90	94510	0.0013	0.67

Table 9. Cost of materials

Materials	Cost (USD/kg)
Ordinary Portland Cement	0.1
Graphene Oxide	16.32
Ground Granulated Blast Furnace Slag	0.15
Water	0.0007
Fine Aggregate	0.02
Coarse Aggregate	0.013
Carboxylate based Super Plasticize	1.6

[DOI: 10.22068/ijmse.2725]

Table 10. Cost analysis of different mixes per m^3 of concrete

Series	Mix	Cost (USD)								Properties		Economic Index	
		GGBFS	GO	OPC	Water	FA	CA	SP	Total Cost	CS	RCP	EI1	EI2
GGBFS	OPC	0	0	42.500	0.119	20.11	8.794	0.068	71.591	43.7	3956	0.610	55.258
	S30	9.562	0	36.125	0.119	20.11	8.794	0.068	77.966	48.7	2745	0.625	35.208
	S40	19.125	0	29.750	0.119	20.11	8.794	0.068	80.091	55.9	2250	0.698	28.093
	S50	28.687	0	23.375	0.119	20.11	8.794	0.068	82.216	50.8	1642	0.618	19.972
	S60	38.250	0	17.000	0.119	20.11	8.794	0.068	84.341	47.9	2270	0.568	26.915
GO-GGBFS	S50-GO0.01	28.687	0.694	23.375	0.119	20.11	8.794	0.068	82.91	53.8	1520	0.649	18.333
	S50-GO0.05	28.687	3.468	23.375	0.119	20.11	8.794	0.068	85.684	58.9	1335	0.687	15.580
	S50-GO0.1	28.687	6.936	23.375	0.119	20.11	8.794	0.068	89.152	63.8	1104	0.716	12.383
	S50-GO0.2	28.687	13.872	23.375	0.119	20.11	8.794	0.068	96.088	57.7	1380	0.600	14.362

OPC: Ordinary Portland Cement,
GO: Graphene Oxide,
GGBFS: Ground Granulated Blast Furnace Slag,
FA: Fine Aggregates,
CA: Coarse Aggregates,
SP: (Carboxylate based) Super Plasticizer,
CS: Compressive Strength,
RCP: Rapid Chloride Permeability,
EI1: The economic Index for Strength,
EI2: The economic Index for Chloride Permeability

- GGBFS and GONPs had a more pronounced role in developing the concrete resistance against chloride penetration and Combined GONPs and GGBFS additions enhanced the resistance to chloride permeation.
- Addition of 0.1 wt.% GO and 50 wt.% GGBFS would increase the compressive strength of the concrete sample up to 42.7% during 28 days and 46% during 90 days compared to OPC. Concrete with a combination of 0.1 wt.% GONPs and 50 wt.% GGBFS witnessed an increase in its flexural strength up to 58.5% during 28 days and 59.2% during 90 days.
- By adding 0.1 wt.% GO and 50 wt.%, concrete chloride permeability decreased substantially 72% for 90-day cured samples compared to OPC.
- GONPs as an alternative to cement up to 0.1% by weight can accelerate the formation of C-S-H gel by increasing the crystalline content of $Ca(OH)_2$, thereby increasing the strength and improving the resistance of water absorption and chloride permeability and corrosion.
- Increased resistance to chloride ion penetration in concrete modified with GO and GGBFS can be attributed to the improvement of pore structure and increase in concrete density. Due to the filling of pores, resistance to chloride ion penetration is improved.
- A significant improvement in corrosion resistance of steel imbedded in concrete has been attained by increasing GONPs and GGBFS.
- The passivity of steel bars increases with the increment of GGBFS up to 50% and GONPs up to 0.1% by weight in the concrete.
- The economic Index for strength and the economic Index for the rapid chloride permeability of 0.1 wt.% GONPs and 50 wt. % GGBFS is more than 1.17 and 4.46 times compared to OPC respectively.

ACKNOWLEDGEMENTS

The authors appreciatively acknowledge the Research Council of Shahid Bahonar University.

ABBREVIATIONS

OPC: Ordinary Portland cement
GONPs: Graphene Oxide Nanoplatelets
GGBFS: Ground Granulated Blast Furnace Slag

[DOI: 10.22068/ijmse.2725]

GO: Graphene Oxide
SCC: Self-Compacting Concrete
HBFC: High Slag Blast Furnace Cement
CH: Hydrated Calcium
C-S-H: Hydrated Calcium Silicate
C-A-H: Hydrated Calcium Aluminate
C3S: Alite (Tricalcium Silicate)
C2S: Belite (Dicalcium Silicate)
C3A: Tricalcium Aluminate
C4AF: Ferro Calcium Aluminate
Aft: Ettringite (Hexacalcium Aluminate Trisulfate Hydrate)
AFm: Calcium Monosulfo-Aluminate
FE-SEM: Field Emission Scanning Electron Microscopy
XRD: X-Ray Diffraction
EDS: Energy-Dispersive X-ray Spectroscopy
XRF: X-ray Fluorescence
FTIR: Fourier Transform Infrared spectroscopy
FA: Fine Aggregates
CA: Coarse Aggregates
SP: (Carboxylate based) Super Plasticizer
CS: Compressive Strength
RCPT: Rapid Chloride Permeability Test
MIP: Mercury Intrusion Porosimetry
TGA: Thermogravimetric analysis
DTG: Differential Thermogravimetric
W/C: Water to Cement Ratio
EIS: Electrochemical Impedance Spectroscopy
R_p: Polarization Resistance of the Reinforcement (Ω)
R_s: Ohmic Resistance in the Electrolyte (Ω)
R_{con}: Structural Resistance of Concrete (Ω)
CPE_{dl}: Constant Phase Element Relative to Reinforcement (F)
CPE_{con}: Constant Phase Element Relative to Concrete (F)
EI1: Economic Index for Strength
EI2: Economic Index for Chloride Permeability

REFERENCES

[1] Hosan, A., Ahmed Shaikh, F., "Compressive Strength Development and Durability Properties Of High Volume Slag and Slag-Fly Ash Blended Concretes Containing Nano-$CaCO_3$", Journal of Materials Research and Technology, 2021, 10, 1310-1322.

[2] Damtoft, J. S., Lukasik, J., Herfort, D., Sorrentino, D., Gartner, E., "Sustainable Development and Climate Change Initiatives", Cement and Concrete Research, 2008, 38, 115-127.

[3] Qu, F., Li, W., Dong, W., Tam, V. W., Yu, T., "Durability Deterioration of Concrete Under Marine Environment From Material to Structure: A Critical Review", Journal of Building Engineering, 2021, 35, (2021), 102074.

[4] Khan, M. U., Ahmad, S., Al-Gahtani, H. J. "Chloride-Induced Corrosion of Steel in Concrete: An Overview on Chloride Diffusion and Prediction of Corrosion Initiation Time", International Journal of Corrosion, 2017, 2017, 5819202.

[5] Martins, A., Carvalho, J., Costa, L., Andrade, H., Melo, T., Ribeiro, J., Pedroti, L., Peixoto, R., "Steel Slags In Cement-Based Composites: An Ultimate Review on Characterization, Applications and Performance", Construction and Building Materials, 2021, 291, 1-19.

[6] Shi, C., Qian, J., "High Performance Cementing Materials from Industrial Slags: A Review", Resources, Conservation and Recycling, 2000, 29, 195-207.

[7] Xiao, B., Wen, Z., Miao, S., Gao, Q., "Utilization of Steel Slag for Cemented Tailings Backfill: Hydration, Strength, Pore Structure, and Cost Analysis", Case Studies in Construction Materials, 2021, 15, e00621.

[8] Shi, H. S., Xu, B. W., Zhou, X. C., "Influence of Mineral Admixtures on Compressive Strength, Gas Permeability and Carbonation of High Performance Concrete", Construction and Building Materials, 2009, 23, 1980-1985.

[9] Zhuang, S., Wang, Q., "Inhibition Mechanisms of Steel Slag on the Early-Age Hydration of Cement", Cement and Concrete Research, 2021, 140, 106283.

[10] Gencel, O., Karadag, O., Oren, O. H., Bilir, T., "Steel Slag and Its Applications in Cement and Concrete Technology: A Review", Construction and Building Materials, 2021, 283, 122783.

[11] Zheng, D., Yang, H., Yu, F., Zhang, B., Cui, H., "Effect of Graphene Oxide on the Crystallization of Calcium Carbonate by C3S Carbonation", Materials, 2019, 12, 2045.

[12] Jiang, Y., Ling, T., Shi, C., Pan. S, "Characteristics of Steel Slags and Their

[DOI: 10.22068/ijmse.2725]

Use in Cement and Concrete—A Review", Resources, Conservation and Recycling, 2018, 136, 187-197.

[13] Özbay, E., Erdemir, M., Durmuş, H. İ., "Utilization and Efficiency of Ground Granulated Blast Furnace Slag on Concrete Properties–A Review", Construction and Building Materials, 2016, 105, 423-434.

[14] Mo, K. H., Alengaram, U. J., Jumaat, M. Z., Yap, S. P., "Feasibility Study of High Volume Slag as Cement Replacement for Sustainable Structural Lightweight Oil Palm Concrete", Journal of Cleaner Production, 2015, 91, 297–304.

[15] Gesoğlu, M., Güneyisi, E., Özbay, E., "Properties of Self-Compacting Concretes Made with Binary, Ternary, and Quaternary Cementitious Blends of Fly Ash, Blast Furnace Slag, and Silica Fume", Construction and Building Materials, 2009, 23, 1847–1854.

[16] Ramezanianpour, A. A., Malhotra, V. M., "Effect of Curing on the Compressive Strength, Resistance to Chloride-Ion Penetration and Porosity of Concretes Incorporating Slag, Fly Ash or Silica Fume", Cement and Concrete Composites, 1995, 17, 125–133.

[17] Bagheri, A. R., Zanganeh, H., Moalemi, M. M., "Mechanical and Durability Properties of Ternary Concretes Containing Silica Fume and Low Reactivity Blast Furnace Slag", Cement and Concrete Composites, 2012, 34, 663–670.

[18] Jau, W. C., Tsay, D. S., "A Study of the Basic Engineering Properties of Slag Cement Concrete and Its Resistance to Seawater Corrosion", Cement and Concrete Research, 1998, 28, 1363–1371.

[19] Hadj-sadok, A., Kenai, S., Courard, L., Darimont, A., "Microstructure and Durability of Mortars Modified with Medium Active Blast Furnace Slag", Construction and Building. Materials, 2011, 25, 1018–1025.

[20] Sengul, O., Tasdemir, M. A., "Compressive Strength and Rapid Chloride Permeability of Concretes with Ground Fly Ash and Slag", Journal of Materials in Civil Engineering, 2009, 21, 494–501.

[21] Yeau, K. Y., Kim, E. K., "An Experimental Study on Corrosion Resistance of Concrete with Ground Granulate Blast-Furnace Slag", Cement and Concrete Research, 2005, 35, 1391–1399.

[22] Cheng, A., Huang, R., Wu, J. K., Chen, C. H., "Influence of GGBS on Durability and Corrosion Behavior of Reinforced Concrete", Materials Chemistry and Physics, 2005, 93, 404–411.

[23] Gupta, S., "Effect of Content and Fineness of Slag as High Volume Cement Replacement on Strength and Durability of Ultra-High Performance Mortar", Journal of Building Materials and Structures, 2016, 3, 43–54.

[24] Dhir, R. K., El-Mohr, M. A. K., Dyer, T. D., "Chloride Binding in GGBS Concrete", Cement and Concrete Research, 1996, 26, 1767–1773.

[25] Berndt, M. L., "Properties of Sustainable Concrete Containing Fly Ash, Slag and Recycled Concrete", Construction and Building Materials, 2009, 23, 2606–2613.

[26] Elahi, A., Basheer, P. A. M., Nanukuttan, S. V., Khan, Q. U. Z., "Mechanical and Durability Properties of High Performance Concretes Containing Supplementary Cementitious Materials", Construction and Building Materials, 2010, 24, 292–299.

[27] Chen, W., Zhu, H., He, Z., Yang, L., Zhao, L. Wen, C., "Experimental Investigation on Chloride-Ion Penetration Resistance of Slag Containing Fiber-Reinforced Concrete under Drying-Wetting Cycles", Construction and Building Materials, 2021, 274, 121829.

[28] Kayali, O., Khan, M. S. H., Sharfuddin Ahmed, M., "The Role of Hydrotalcite in Chloride Binding and Corrosion Protection in Concretes with Ground Granulated Blast Furnace Slag", Cement and Concrete Composites, 2012, 34, 936–945.

[29] Sideris, K. K., Tassos, C., Chatzopoulos, A., Manita, P., "Mechanical Characteristics and Durability of Self-Compacting Concretes Produced with Ladle Furnace Slag", Construction and Building Materials, 2018, 170, 660–667.

[30] Irico, S., Qvaeschning, D., Mutke, S., Deuse, T., Gastaldi, D., Canonico, F., "Durability of High Performance Self-Compacting Concrete with Granulometrically Optimized Slag

[DOI: 10.22068/ijmse.2725]

Cement", Construction and Building Materials, 2021, 298, 1-9.
[31] Thomas, M. D., Scott, A., Bremner, T., Bilodeau, A., Day, D., "Performance of Slag Concrete in Marine Environment", ACI Materials Journal, 2008, 105, 628–634.
[32] McNally, C., Sheils, E., "Probability-Based Assessment of the Durability Characteristics of Concretes Manufactured Using CEM II and GGBS Binders", Construction and Building Materials, 2012, 30, 22–29.
[33] Fraj, A.B., Bonnet, S., Leklou, N., Khelidj, A., "Investigating the Early-Age Diffusion of Chloride Ions in Hardening Slag-Blended Mortars on The Light of Their Hydration Progress", Construction and Building Materials, 2019, 225, 485–495.
[34] Duraman, S. B., Richardson, I. G., "Microstructure & Properties of Steel-Reinforced Concrete Incorporating Portland Cement and Ground Granulated Blast Furnace Slag Hydrated at 20 °C", Cement and Concrete Research, 2020, 137, 2-12.
[35] Zhuang, S., Wang, Q., "Inhibition Mechanisms of Steel Slag on the Early-Age Hydration of Cement", Cement and Concrete Research, 2021, 140, 1-14.
[36] Aprianti, E., Shafigh, P., Zawawi, R., Abu Hassan, Z. F., "Introducing an Effective Curing Method for Mortar Containing High Volume Cementitious Materials", Construction and Building Materials, 2016, 107, 365–377.
[37] Megat Johari, M. A., Brooks, J. J., Kabir, S., Rivard, P., "Influence of Supplementary Cementitious Materials on Engineering Properties of High Strength Concrete", Construction and Building Materials, 2011, 25, 2639–2648.
[38] Sadawy, M.M., Nooman, M.T., "Influence of Nano-Blast Furnace Slag on Microstructure, Mechanical and Corrosion Characteristics of Concrete", Materials Chemistry and Physics, 2020, 251, 1-12.
[39] Rajamallu, C., Chandrasekhar Reddy, T., Arunakanthi E., "Service Life Prediction of Self-Compacted Concretes with Respect to Chloride Ion Penetration", Materials Today: Proceedings, 2020, 1-5.
[40] Han, X., Feng, J., Shao, Y., Hong, R., "Influence of a Steel Slag Powder-Ground Fly Ash Composite Supplementary Cementitious Material on the Chloride and Sulphate Resistance of Mass Concrete", Powder Technology, 2020. 370, 176–183.
[41] Fan, J., Zhu, H., Shi, J., Li, Z., Yang, S., "Influence of Slag Content on The Bond Strength, Chloride Penetration Resistance, and Interface Phase Evolution of Concrete Repaired with Alkali Activated Slag/Fly Ash", Construction and Building Materials, 2020, 263, 120639.
[42] Ali-Boucetta, T., Behim, M., Cassagnabere, F., Mouret, M., Ayat, A., Laifa, W., "Durability of Concrete Containing GGBFS And GO Containing Waste Bottle Glass and Granulated Slag", Construction and Building Materials, 2021, 270, 121133.
[43] Park, J. S., Yoon, Y. S., Kwon, S. J., "Strength and Resistance to Chloride Penetration in Concrete Containing GBFS with Ages", Journal of the Korea Concrete Institute, 2017, 29, 307-314.
[44] Du, H., Gao, H. J., Dai Pang, S., "Improvement in Concrete Resistance Against Water and Chloride Ingress by Adding Graphene Nanoplatelet", Cement and Concrete Research, 2016, 83, 114-123.
[45] Wu, Z., Shi, C., Khayat, K. H., "Influence of Silica Fume Content on Microstructure Development and Bond to Steel Fiber in Ultra-High Strength Cement-Based Materials (UHSC)", Cement and Concrete Composites, 2016, 71, 97-109.
[46] Samad, S., Shah, A., Limbachiya, M. C., "Strength Development Characteristics of Concrete Produced with Blended Cement Using Ground Granulated Blast Furnace Slag (GGBS) under Various Curing Conditions", Sādhanā, 2017, 42, 1203-1213.
[47] Gesoğlu, M., Özbay, E., "Effects of Mineral Admixtures on Fresh and Hardened Properties of Self-Compacting Concretes: Binary, Ternary and Quaternary Systems", Materials and Structures, 2007, 40, 923-937.
[48] Ying, J., Zhou, B., Xiao J., "Pore Structure and Chloride Diffusivity of Recycled Aggregate Concrete with Nano-SiO_2 and

[DOI: 10.22068/ijmse.2725]

Nano-TiO_2", Construction and Building Materials, 2017, 150, 49–55.

[49] Chuah S., Pan Z., Sanjayan J. G., Wang C. M., Duan W. H., "Nano Reinforced Cement and Concrete Composites and New Perspective from Graphene Oxide", Construction and Building Materials, 2014, 73, 113–124.

[50] Yuan, X. Y., Zeng, J. J., Niu, J. W., Qin, Z., "Effect of Different Water-Reducing Agents on Mechanical Properties and Microstructure of Graphite Oxide-Blended Cement Mortar", Journal of Functional Materials, 2018, 49, 10184-10189.

[51] Devasena, M., Karthikeyan, J., "Investigation on Strength Properties of Graphene Oxide Concrete", International Journal of Engineering Science Invention Research & Development, 2015, 1, 307-310.

[52] Wang, Q., Wang, J., Lu, C. X., Liu, B. W., Zhang, K., Li, C. Z., "Influence of Graphene Oxide Additions on the Microstructure and Mechanical Strength of Cement", New Carbon Materials, 2015, 30, 349-356.

[53] Lua, Z., Li, X., Hanif, A., Chen, B., Parthasarathy, P., Yu, J., Li, Z., "Early-Age Interaction Mechanism Between the Graphene Oxide and Cement Hydrates", Construction and Building Materials, 2017, 152, 232-239.

[54] Hou, D., Lu, Z., Li, X., Ma, H., Li, Z., "Reactive Molecular Dynamics and Experimental Study of Graphene-Cement Composites: Structure, Dynamics and Reinforcement Mechanisms", Carbon, 2017, 115, 188-208.

[55] Long, W. J., Wei, J. J., Xing, F., Khayat, K. H., "Enhanced Dynamic Mechanical Properties of Cement Paste Modified with Graphene Oxide Nanosheets and Its Reinforcing Mechanism", Cement and Concrete Composites, 2018, 93, 127-139.

[56] Jing, G., Wu, J., Lei, T., Wang, S., Strokova, V., Nelyubova, V., Wang, M., Ye, Z., "From Graphene Oxide to Reduced Graphene Oxide: Enhanced Hydration and Compressive Strength of Cement Composites", Construction and Building Materials, 2020, 248, 1-9.

[57] Yang, H., Monasterio, M., Cui, H., Han, N., "Experimental Study of the Effects of Graphene Oxide on Microstructure and Properties of Cement Paste Composite", Composites Part A: Applied Science and Manufacturing, 2017, 102, 263-272.

[58] Lv, S., Ma, Y., Qiu, C., Sun, T., Liu, J., Zhou, Q., "Effect of Graphene Oxide Nanosheets of Microstructure and Mechanical Properties of Cement Composites", Construction and Building Materials, 2013, 49, 121-127.

[59] Peng H., Ge, Y., Cai, C.S., Zhang, Y., Zhen Liu, "Mechanical Properties and Microstructure of Graphene Oxide Cement-Based Composites", Construction and Building Materials, 2019, 194, 102–109.

[60] Somasri, M., Kumar, B. N., "Graphene Oxide as Nano Material in High Strength Self-Compacting Concrete", Materials Today: Proceedings, 2021, 43, 2280–2289.

[61] Wang, Y., Yang, J., Ouyang, D., "Effect of Graphene Oxide on Mechanical Properties of Cement Mortar and It's Strengthening Mechanism", Materials, 2019, 12, 1-18.

[62] Zhu, X. H., Kang, X. J., Yang, K., Yang, C. H., "Effect of Graphene Oxide on the Mechanical Properties and the Formation of Layered Double Hydroxides (LDHs) in Alkali-Activated Slag Cement", Construction and Building Materials, 2017, 132, 290–295.

[63] Lyu, S. H., Sun, T., Liu, J. J., Ma, Y. J., Qiu, C. C., "Toughening Effect and Mechanism of Graphene Oxide Nanosheets on Cement Matrix Composites", Acta Materiae Compositae Sinica, 2014, 31, 644-652.

[64] Mohammed, A., Sanjayan, J. G., Duan, W. H., Nazari, A., "Graphene Oxide Impact on Hardened Cement Expressed in Enhanced Freeze-Thaw Resistance", Journal of Materials in Civil Engineering, 2016, 28, 04016072.

[65] Wang, Q., Li, S., Pan, S., Cui, X., Corr, D. J., Shah, S. P., "Effect of Graphene Oxide on the Hydration and Microstructure of Fly Ash-Cement System", Construction and Building Materials, 2019, 198, 106-119.

[66] Jiang, W., Li, X., Lv, Y., Zhou, M., Liu, Z., Ren, Z., Yu, Z., "Cement-Based Materials Containing Graphene Oxide and Polyvinyl

[DOI: 10.22068/ijmse.2725]

Alcohol Fiber: Mechanical Properties, Durability, and Microstructure", Nanomaterials, 2018, 8, 638.
[67] Bhojaraju, C., Mousavi, S. S., Brial, V., DiMare, M., Ouellet-Plamondon, C. M., "Fresh and Hardened Properties of Ggbs-Contained Cementitious Composites Using Graphene and Graphene Oxide", Construction and Building Materials, 2021, 300, 1-18.
[68] Li, X., Korayem A. H., Li C., Liu Y., He H., Sanjayan J. G., Duan W.H., "Incorporation of Graphene Oxide and Silica Fume into Cement Paste: A Study of Dispersion and Compressive Strength", Construction and Building Materials, 2016, 123, 327–335.
[69] Xu, G., Zhong, J., Shia, X., "Influence of Graphene Oxide in a Chemically Activated Fly Ash", Fuel, 2018, 226, 644–657.
[70] Vishnu, N., Kolli, R., Ravella, D. P., "Studies on Self-Compacting Geopolymer Concrete Containing Flyash, GGBS, Wollastonite and Graphene Oxide", Materials Today: Proceedings, 2021, 43, 2422–2427.
[71] Sharma, S., Kothiyal, N. C., "Comparative Effects of Pristine and Ball-Milled Graphene Oxide on Physico-Chemical Characteristics of Cement Mortar Nanocomposites", Construction and Building Materials, 2016, 115, 256–268.
[72] ASTM C150, Standard Specification for Portland cement Annual Book of ASTM Standards, ASTM, Philadelphia, PA, 2017.
[73] Lu, L., Ouyang, D., "Properties of Cement Mortar and Ultra-High Strength Concrete Incorporating Graphene Oxide Nanosheets", Nanomaterials, 2017, 7, 187.
[74] Siburian, R., Sihotang, H., Raja, S. L., Supeno, M., Simanjuntak, C., "New Route to Synthesize of Graphene Nano Sheets", Oriental Journal of Chemistry, 2018, 34, 182.
[75] Storm, M. M., Johnsen, R. E., Norby, P., "In Situ X-Ray Powder Diffraction Studies of the Synthesis of Graphene Oxide and Formation of Reduced Graphene Oxide", Journal of Solid State Chemistry, 2016, 240, 49-54.
[76] Ahmad, A., Ullah, S., Khan, A., Ahmad, W., Khan, A. U., Khan, U. A., Rahman, A. U., Yuan, Q., "Graphene Oxide Selenium Nanorod Composite as a Stable Electrode Material for Energy Storage Devices", Applied Nanoscience, 2020, 10, 1243-1255.
[77] ASTM C192M-16a, Standard Practice for Making and Curing Concrete Test Specimens in the Laboratory, ASTM International, West Conshohocken, PA, USA, 2016.
[78] ASTM C39, Standard Test Method for Compressive Strength of Cylindrical Concrete Specimens, ASTM, Philadelphia, PA, 2017.
[79] ASTM C293, Standard Test Method for Flexural Strength of Concrete (Using Simple Beam with Center-Point Loading), ASTM, Philadelphia, PA, 2017.
[80] ASTM C496, Standard Test Method for Splitting Tensile Strength of Cylindrical Concrete Specimens, ASTM, Philadelphia, PA, 2017.
[81] ASTM C1202-12,, Standard Test Method for Electrical Indication of Concrete's Ability to Resist Chloride Ion Penetration, ASTM International, West Conshohocken, PA, USA, 2012.
[82] Lataste, J. F., Sirieix, C., Breysse, D., Frappa, M., "Electrical Resistivity Measurement Applied to Cracking Assessment on Reinforced Concrete Structures in Civil Engineering", NDT & E International, 2003, 36, 383-394.
[83] Azarsa, P., Gupta, R., "Electrical Resistivity of Concrete for Durability Evaluation: A Review", Advances in Materials Science and Engineering, 2017, 2017, 8453095.
[84] ASTM C642, Standard Test Method for Density, Absorption, and Voids in Hardened Concrete, ASTM, Philadelphia, PA, 2013.
[85] ASTM C1679-08, Standard Practice for Measuring Hydration Kinetics of Hydraulic Cementitious Mixtures Using Isothermal Calorimetry, ASTM, Philadelphia, PA, 2008.
[86] ASTM D4404, Standard Test Method for Determination of Pore Volume and Pore Volume Distribution of Soil and Rock by Mercury Intrusion Porosimetry, ASTM, Philadelphia, PA, 2010.

[DOI: 10.22068/ijmse.2725]

[87] ASTM C1872-18, Standard Test Method for Thermogravimetric Analysis of Hydraulic Cement, ASTM International, West Conshohocken, PA, 2018.
[88] Shen, D., Jiao, Y., Kang, J., Feng, Z., Shen, Y., "Influence of Ground Granulated Blast Furnace Slag on The Early-Age Cracking Potential of Internally Cured High-Performance Concrete", Construction and Building Materials, 2020, 233, 117083.
[89] Güneyisi, E., Gesoğlu, M., "A Study on Durability Properties of High-Performance Concretes Incorporating High Replacement Levels of Slag", Materials and Structures, 2008, 41, 479-493.
[90] Park, J-H., Lee, H-S., "Effect of Curing Condition on The Chloride Ion Diffusion Coefficient in Concrete with GGBFS", Journal of the Korea Institute of Building Construction, 2019, 19, 421-429.
[91] Yoon, Y-S., Cho, S-J., Kwon, S-J., "Prediction Equation for Chloride Diffusion in Concrete Containing GGBFS Based on 2-Year Cured Results", Journal of the Korea institute for structural maintenance and inspection, 2019, 23, 1-9.
[92] Yang, H-M., Kwon, S-J., Myung, NV,, Singh, JK., Lee, H-S., Mandal, S., "Evaluation of Strength Development in Concrete with Ground Granulated Blast Furnace Slag Using Apparent Activation Energy", Materials, 2020, 13, 442.
[93] Oner, A., Akyuz, S., "An Experimental Study on Optimum Usage of GGBS for the Compressive Strength of Concrete", Cement and Concrete Composites, 2007, 29, 505-514.
[94] Gong, K., Pan, Z., Korayem, A. H., Qiu, L., "Reinforcing Effects of Graphene Oxide on Portland Cement Paste", Journal of Materials in Civil Engineering, 2014, 27, A4014010.
[95] Li, S., Liu, G., Yu, Q., "The Role of Carbonated Steel Slag on Mechanical Performance of Ultra-High Performance Concrete Containing Coarse Aggregates", Construction and Building Materials, 2021, 307, 124903.
[96] Li, P., Brouwers, H., Chen, W., Yu, Q., "Optimization and Characterization of High-Volume Limestone Powder in Sustainable Ultra-High Performance Concrete", Construction and Building Materials, 2020, 242, 118112.
[97] Huang, W., Kazemi-Kamyab, H., Sun, W., Scrivener, K., "Effect of Cement Substitution by Limestone on the Hydration and Microstructural Development of Ultra-High Performance Concrete (UHPC)", Cement Concrete Composites, 2017, 77, 86–101.
[98] Mahendran, R., Sridharan, D., Santhakumar, K., Selvakuma,r T., Rajasekar, P., Jang, J-H., "Graphene Oxide Reinforced Polycarbonate Nanocomposite Films with Antibacterial Properties", Indian Journal of Materials Science, 2016, 1-10.
[99] Jang, S., Karthick, S., Kwon, S., "Investigation on Durability Performance in Early Aged High-Performance Concrete Containing GGBFS and FA", Advances in Materials Science and Engineering, 2017, 1-11.
[100] Guo, K., Miao, H., Liu, L., Zhou, J., Liu, M., "Effect of Graphene Oxide on Chloride Penetration Resistance of Recycled Concrete", Nanotechnology Reviews, 2019, 8, 681–689.
[101] Kumar, R., Bhattacharjee, B., "Porosity, Pore Size Distribution and in Situ Strength of Concrete", Cement and Concrete Research, 2003, 33, 155-164.
[102] Ye, G., Xiu, X., De Schutter G., Poppe A.M., Taerwe L., "Influence of Limestone Powder Used as Filler in SCC on Hydration and Microstructure of Cement Pastes", Cement and Concrete Composites, 2007, 29, 94–102.
[103] Polder, R.B., De Rooij, M.R., "Durability of Marine Concrete Structures – Field Investigations and Modelling", Heron, 2005, 50, 133-153.
[104] Dai, J., "The Effect of Fineness on the Hydration Activity Index of Ground Granulated Blast Furnace Slag", Materials, 2019, 12.
[105] Li, X., Liu, Y. M., Li, W.G., Li, C.Y., Sanjayan, J.G., Duan, W.H., Li, Z., "Effects of Graphene Oxide Agglomerates on Workability, Hydration, Microstructure and Compressive Strength of Cement Paste", Construction and Building Materials, 2017, 145, 402-410.

[DOI: 10.22068/ijmse.2725]

[106] Li, M., Kim, J.M., "Strength Properties and Micro-Structure of Steel Slag Based Hardened Cementitious Composite with Graphene Oxide", MATEC Web of Conferences, EDP Sciences, 2017.
[107] Yu, L., Jiang, L., Chu, H., Guo, M., Zhu, Z., Dong, H., "Effect of Electrochemical Chloride Removal and Ground Granulated Blast Furnace Slag on the Chloride Binding of Cement Paste Subjected to NaCl and Na_2SO_4 Attack", Construction and Building Materials, 2019, 220, 538-546.
[108] Luo, R., Cai, Y., Wang, C., Huang, X., "Study of Chloride Binding and Diffusion in GGBS Concrete", Cement and Concrete Research, 2003, 33, 1-7.
[109] Khan, M., Kayali, O., "Chloride Binding Ability and the Onset Corrosion Threat on Alkali-Activated GGBFS and Binary Blend Pastes", European Journal of Environmental and Civil Engineering, 2018, 22, 1023-1039.
[110] Long, W., "Electrochemical Characterization and Inhibiting Mechanism on Calcium Leaching of Graphene Oxide Reinforced Cement Composites", Nanomaterials, 2019, 9, 1-19.

[DOI: 10.22068/ijmse.2725]